

pubs.acs.org/NanoLett Letter

Anapole-Assisted Low-Power Optical Trapping of Nanoscale Extracellular Vesicles and Particles

Ikjun Hong, Chuchuan Hong, Oleg S. Tutanov, Clark Massick, Mark Castleberry, Qin Zhang, Dennis K. Jeppesen, James N. Higginbotham, Jeffrey L. Franklin, Kasey Vickers, Robert J. Coffey, and Justus C. Ndukaife*



Cite This: Nano Lett. 2023, 23, 7500-7507



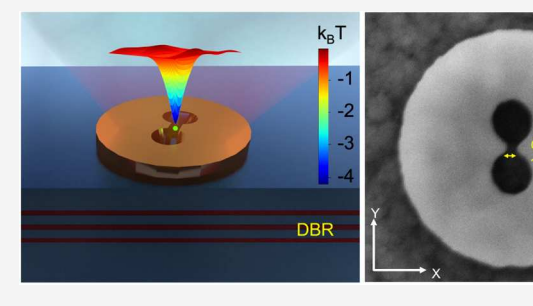
ACCESS

Metrics & More



Supporting Information

ABSTRACT: This study addresses the challenge of trapping nanoscale biological particles using optical tweezers without the photothermal heating effect and the limitation presented by the diffraction limit. Optical tweezers are effective for trapping microscopic biological objects but not for nanoscale specimens due to the diffraction limit. To overcome this, we present an approach that uses optical anapole states in all-dielectric nanoantenna systems on distributed Bragg reflector substrates to generate strong optical gradient force and potential on nanoscale biological objects with negligible temperature rise below 1 K. The anapole antenna condenses the accessible electromagnetic energy



to scales as small as 30 nm. Using this approach, we successfully trapped nanosized extracellular vesicles and supermeres (approximately 25 nm in size) using low laser power of only 10.8 mW. This nanoscale optical trapping platform has great potential for single molecule analysis while precluding photothermal degradation.

KEYWORDS: Anapole, nanotweezer, extracellular vesicles, supermeres, electric field enhancement, distributed Bragg reflector

o generate strong optical gradient forces in an optical tweezer, the trapping laser must be focused to tight focal spots. Unfortunately, the diffraction limit of light precludes focusing light to nanoscale volumes below the diffraction limit. This poses a major challenge in addressing nanoscale biological particles using optical tweezers. In the quasi-static limit, when the size of the particle is much smaller than the wavelength of light, the optical gradient force scales as the volume of the particle, making it necessary to use high optical powers to trap nanoscale objects. For example, the stable trapping of nanoscale extracellular vesicles (EVs) in an optical trap requires more than 100 mW of input optical power, which often predisposes them to photothermal damage. 1-3 Of interest is to develop novel optical nanotweezers that can confine light to nanoscale volumes well below the diffraction limit to enable low laser power trapping while utilizing laser sources in the near-infrared biological transparency window, which range from 800 to 1200 nm. Addressing this challenge is key to developing new optical trapping technologies for the stable trapping and study of nanoscale EVs and nonvesicular extracellular nanoparticle (NVEP) in solution, which are generating substantial scientific interest. Extracelluar vesicles and particles (EVPs), which are nanoscale particles that include EVs and NVEPs, are secreted by virtually all cells and have been identified as an important means for cells to communicate with neighboring or distant cells.⁴ Small EVs

contain molecular cargos such as nucleic acids, proteins, and lipids and serve as a means for cells to communicate with neighboring or distant cells. ^{4,5} In addition, newly discovered NVEPs known as exomeres and supermeres that are only ~35 nm and ~25 nm in size, respectively, have also been reported. Supermeres are found to be replete with disease biomarkers and possess a marked ability to cross the bloodbrain barrier. Their small sizes, which are substantially smaller than the wavelength of light at optical frequencies, make them even more challenging to be trapped with the conventional optical tweezers.

Over the years, several light-based tools known as optical nanotweezers have been investigated for confining light to nanoscale spots toward the optical trapping of nanoscale objects. These tools include plasmonic nanotweezers where plasmonic nanostructures usually made of gold are used to confine light to the deeply subwavelength scales to enhance the optical gradient force. Though plasmonic

Received: May 30, 2023 Revised: July 17, 2023 Published: August 8, 2023





Nano Letters pubs.acs.org/NanoLett Letter

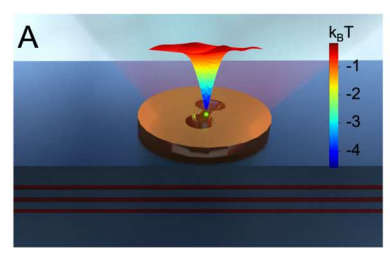
nanoantennas can enhance the local light intensity by 2-3 orders of magnitude relative to the incident light intensity, they have intrinsic optical loss that results in photothermal heating effects^{15–17} which must be managed. To circumvent the issue of loss in plasmonic systems, all-dielectric optical nanoantenna supporting Mie resonances have also been investigated but they produce modest electromagnetic field enhancement factors of approximately 5 times (i.e., intensity enhancement of 25 times), 18 an order of magnitude lower than their plasmonic counterparts. It is noteworthy that Jiang et al. demonstrated that the thermal effect in plasmonic system can rather enhance the stiffness of the trapped particles in surfactant-containing medium, exhibiting thermophilic behavior. 19 However, in the absence of surfactants, the thermophoretic force is repulsive and works to preclude trapping.²⁰ Nanoscale optical trapping based on quasi-BIC has also been proposed but it provided multiple hot spots that are better suited for multiple particle trapping.²¹

Here, we experimentally demonstrate a new approach for optical trapping at the nanoscale by harnessing the anapole states of light in all-dielectric nanoantenna systems for the first time. Optical anapole states result from the interference between electric and toroidal dipole resonance²²⁻²⁵ and provide a new means to confine and enhance the light field in all-dielectric nanostructures. Our proposed anapole nanotweezer (ANT) harnesses the optical anapole states to confine light to the nanoscale and generate an enhanced optical gradient force on nanoscale NVEPs. We note that optical anapoles are actively investigated for optoelectronic applications such as anapole lasers²⁶ and for second-harmonic generation²⁷ due to their highly enhanced fields. While nearfield optical trapping using anapole states have been theoretically proposed by us and others, no experimental demonstration has been reported to date.²⁸⁻³¹ The electromagnetic energy inside the anapole disk is not accessible because most of the light field is trapped within the dielectric nanodisk antenna supporting the anapole states. To make the field accessible to nearby biological molecules for near-field trapping, we introduced a double-nanohole slot at the center of the anapole disk. In addition to making the enhanced electromagnetic field accessible, the double nanohole enhances the optical field due to the slot effect provided by the continuity of the normal component of the displacement field and enables the spatial confinement of the enhanced field in the x-y plane. The mode volume within the double-nanohole is comparable to the physical size of the nanoscale particle, providing a significant advantage in the trapping and analysis of single nanoscale particles.

The anapole antenna comprises a silicon disk on a substrate. To increase the electromagnetic field enhancement factor, the anapole antenna is placed on a distributed Bragg reflector (DBR) with a designed spacer layer to support second order anapole state near the 973 nm wavelength. The result in Figure S1 shows that the DBR with three pairs of Si and SiO₂ layers was sufficient to reflect about 95% of incident photons near 973 nm wavelength. To optimize the field enhancement of the anapole antenna, a layer of SiO₂ with 250 nm thickness was deposited onto the DBR. This additional space layer was chosen to optimize the interaction of the anapole nanoantenna with the incident light and double the amplitude of the background electric field when compared to the amplitude of the incident electric field, as illustrated in Figure S2. This spacer layer thickness ensures that the position of the anapole

antenna is at the center of the peak of the background electric field as shown in Figure S2A.

The optimized radius and height of the designed anapole disk are selected to be 455 nm and 130 nm, respectively, as shown in Figure S3. The gap size of the DNH is \sim 30 nm along the x direction, as shown in Figure 1B. The laser to excite the



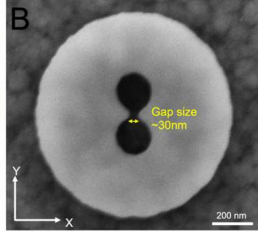


Figure 1. Designed and fabricated anapole nanoantenna on a distributed Bragg reflector. (A) Illustration of the designed anapole with an estimated potential well showing $\sim \! 4.6 k_{\rm B} T$ for a 50 nm extracellular vesicle (EV) under 19 mW. (B) SEM image of fabricated anapole with double nanohole aperture.

anapole has a 973 nm wavelength with the polarization along the x direction. All the materials for the trapping system, including DI water, SiO_2 , and Si, have a negligible loss at 973 nm wavelength.

The electromagnetic near-field profiles of the anapole state are displayed in Figure 2A,B. The maximum electric field enhancement $(|E|/|E_0|)$ is as high as ~41 times (which corresponds to an intensity enhancement of about 1600 times), located in the DNH slot, as shown in Figure 2A. The field is tightly confined along the x and y directions by optimizing the center-to-center distance of the DNH as described in Figure S5. This field enhancement is an order of magnitude higher than in Mie-resonant dielectric nanoantenna.³² The high intensity enhancement and spatial field confinement of this optical anapole antenna system are crucial to generating strong optical force on nanoscale biological objects with low laser power. Figure 2B shows the field profile on the xz cross-section plane along the middle of the silicon disk. The field penetrates inside the adjoining fluid medium and is accessible to the particles in the medium. Figure 2C indicates that the field enhancement on a glass substrate without the use of the designed DBR reflector is only enhanced by a factor of 16 times. The field distributions in Figure 2A (anapole on DBR) and Figure 2C (anapole on glass substrate) are similar, and it is noteworthy that the excited anapole can support a much higher field enhancement by employing the DBR layer relative to the glass substrate. The calculated scattering cross-section with the electric field enhancement is plotted in Figure 2D. The scattering is suppressed at the anapole state, where the electric field enhancement is maximized. We measured the scattering spectrum of the fabricated anapole antenna using a homemade dark-field setup, and we observed the dip in the spectrum as expected. Figure 2E shows the simulated and measured scattering spectra, which depict a good match between simulation and experimental data. The supercontinuum source with a condenser was used to collect only the scattered light from the anapole antenna, as described in Figure S6. Thermal simulation was performed to verify the negligible temperature rise from the anapole antenna on a DBR system. The thermal simulation was performed by coupling the wave-optics module with the heat transfer module

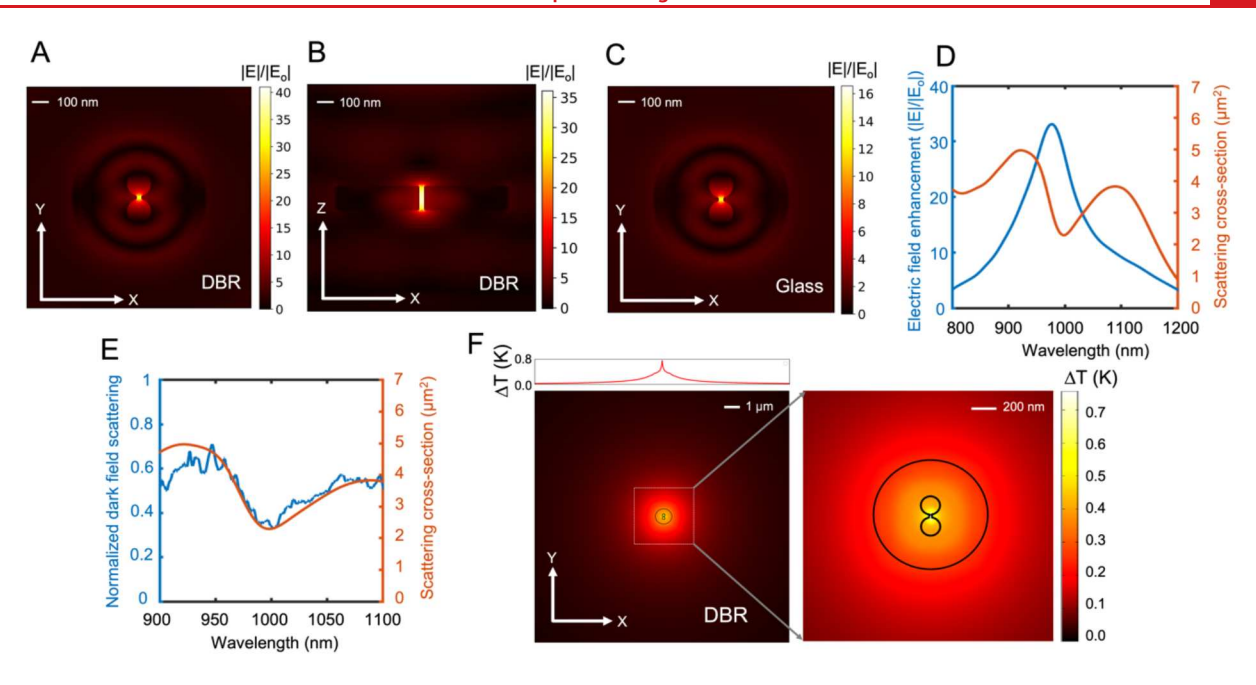


Figure 2. Excitation of anapole state with electric field distribution at a wavelength of 973 nm. (A) Distribution of electric field enhancement along the XY plane, at 65 nm above the DBR reflector. (B) Distribution of electric field enhancement along the XZ plane, at middle of the anapole disk on the DBR system. (C) Distribution of field enhancement along the XY plane for anapole disk on glass substrate. (D) Scattering cross-section with electric field enhancement when the radius and height of anapole nanoantenna are 455 and 130 nm, respectively. (E) Measured dark-field scattering matches well with the simulation result. (F) The results of the thermal simulation show that the maximum temperature rise is only \sim 0.75 K along the XY plane.

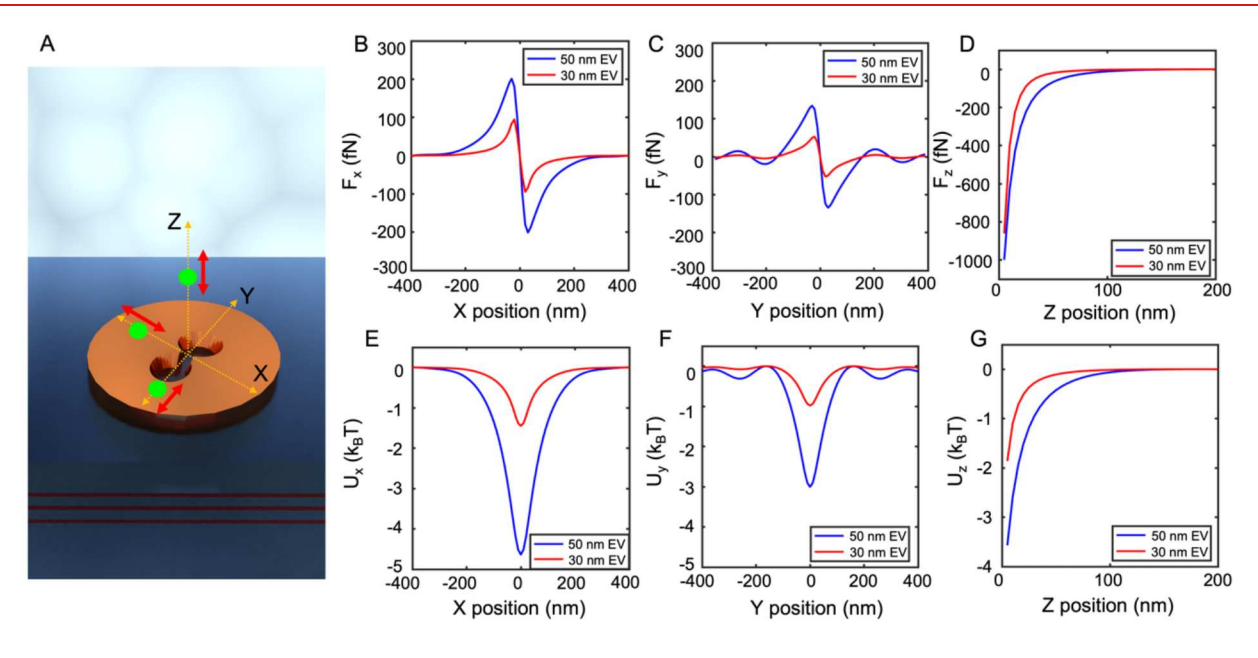


Figure 3. Calculation of optical trapping force and potential for 50 and 30 nm EV. (A) Particle trajectories during the MST calculation along the x, y, or z direction. (B, E) Calculated optical force (Fx) on a particle with the corresponding potential energy. (C, F) Calculated optical force (Fy) on a particle with the corresponding potential energy. (D, G) Calculated optical force (Fz) with the corresponding potential energy (Uz).

in the COMSOL Multiphysics software package as detailed in section S4. The measured optical properties of the silicon from ellipsometry measurements were utilized for the simulation model as described in Figure S7 and the extinction coefficient (κ) of water at 973 nm wavelength was taken as 0.000 003 4.³³ When the power of the laser is set as 19 mW with a 1.33 μ m spot size in diameter, the maximum temperature rise was found to be approximately 0.75 K at 973 nm wavelength, as shown in

Figure 2F. The negligible increase in temperature implies that the anapole excitation does not result in increased Brownian motion, thermophoretic particle movement, or buoyancy-driven thermal convection while boosting the electric field enhancement. Thus, the nanoscale optical trapping force is primarily due to the anapole-enhanced near-field optical gradient force. We calculated the optical force by employing the Maxwell's stress tensor (MST) formalism.³⁴

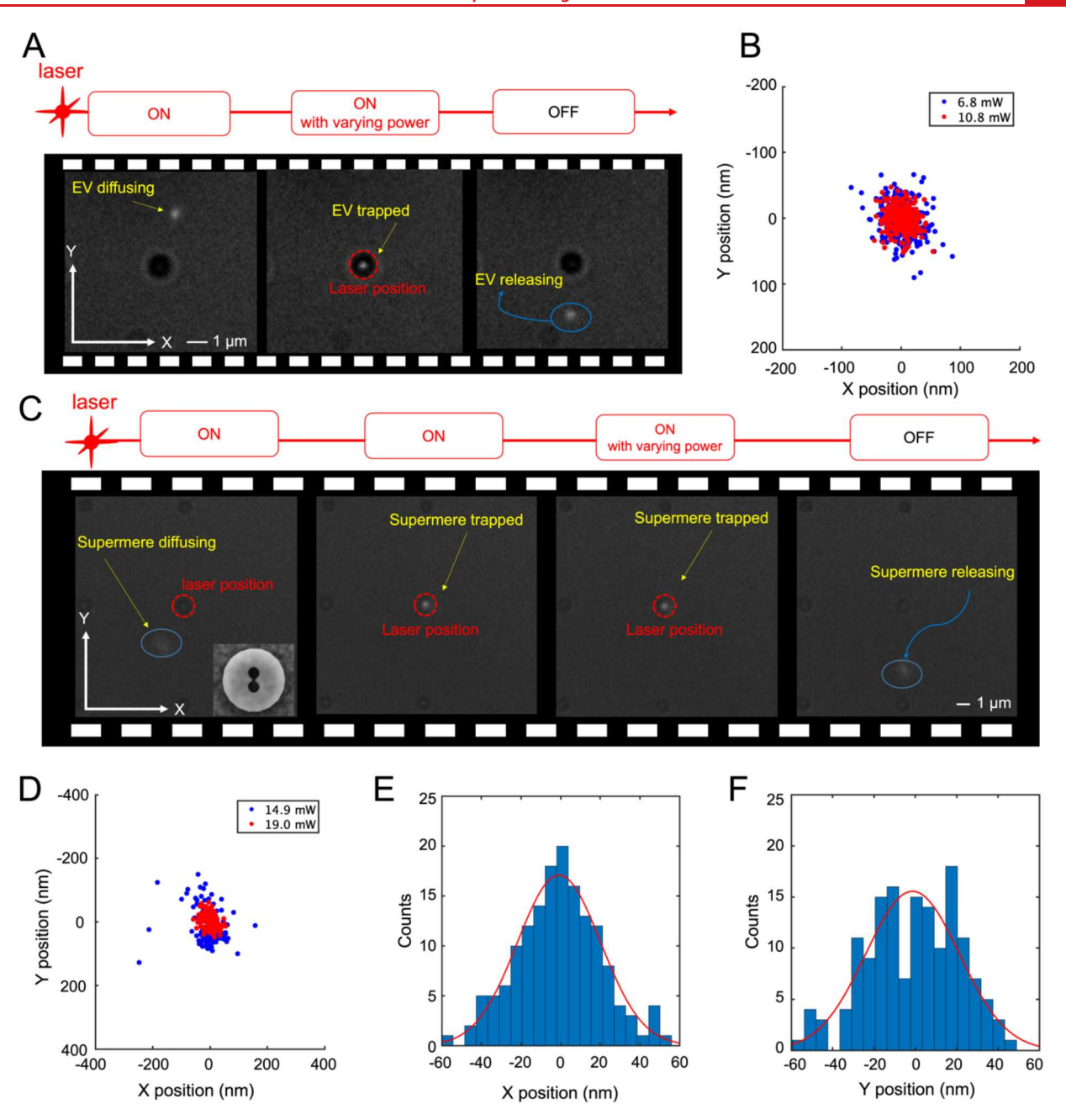


Figure 4. EV and supermere trapping experiments. (A) The EV trapping experiment shows that the diffusing EV is trapped on the anapole nanoantenna, and then the EV is released when the 973 nm laser is turned off. (B) The scatter plot shows the EV's trajectory when the EV is trapped on the anapole nanoantenna. The highest estimated stiffness along the x- and y-axis is 0.347 fN/nm and 0.329 fN/nm under 10.8 mW incident laser power, respectively. (C) The frame sequence of supermere trapping experiment shows how the diffusing supermere is trapped near the anapole nanoantenna until the laser is off. (D) The scatter plot shows the supermere's trajectory when the supermere is trapped at the anapole structure. The estimated stiffness for the trapped supermere under 19 mW incidence along the x- and y-axis are 0.215 fN/nm and 0.205 fN/nm, respectively. (E, F) Histogram of the trapped supermere particle's position under 19 mW incident laser power along x and y directions, respectively. The red curve is the Gaussian fitting to estimate the trap stiffness.

In the MST formalism, the optical force on a particle is determined by integrating the stress tensor over an arbitrary surface enclosing the particle, as described in section S8. We calculate the optical force and trapping potential along the x, y, and z directions by assuming vesicles with sizes of 50 and 30 nm, which is within the lower range of size corresponding to small EVs. According to the guidelines of the International Society of Extracellular Vesicles (ISEV), small EVs are categorized as EVs that are less than 200 nm in size. This prior reports show that the refractive index of EVs are heteroge-

neous and range from 1.37 to 1.39.³⁶ For the purpose of the numerical simulations, we set the refractive index of the particle as 1.39. The laser power and spot size of the laser were set as 19 mW and 1.33 μ m², respectively. Figure 3B shows the calculated *x*-component of the optical force along the *x*-axis when an EV is positioned along the *x*-axis. For the optical force simulations, the position of the lowest point on the EV surface is assumed to be 5 nm above the anapole disk. The optical force is always pointing toward the center of a slot. Figure 3E depicts the trapping potential along the *x* directions, showing a

Nano Letters pubs.acs.org/NanoLett Letter

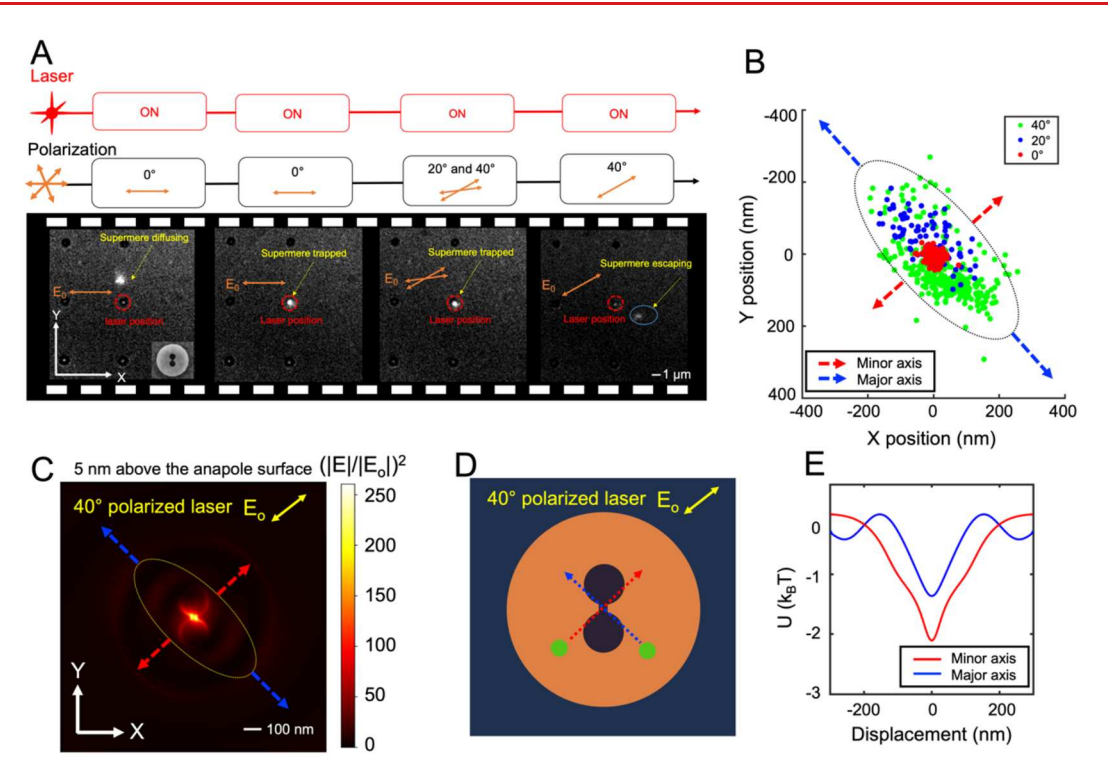


Figure 5. Supermere trapping experiments under varying polarization of incident laser. (A) The supermere trapping experiment shows that the diffusing supermere is trapped on the anapole nanoantenna, and then the polarization is changed from 0° to 40° . (B) Scatter plot showing the trajectory of the supermere when the incident laser polarization is changed. (C) Intensity enhancement distribution when the polarization of the incident laser is at an angle of 40° from the *x*-axis. Note that there is a larger gradient along the direction represented as minor axis than along the major axis shown in the figure. (D) The *XY*-plane schematic shows the particle's position for the MST calculations used to compare the trapping potential well along with a major and minor axis, indicated as blue and red arrows, respectively. Two green circles indicate a bioparticle. (E) Calculated optical potential shows a different level of potential depth.

potential of \sim 4.6 k_BT and 1.4 k_BT for a 50 and 30 nm EV, respectively. Figure 3C and Figure 3F show the results of the optical force and corresponding potential energy along the yaxis when the particle is 5 nm above the anapole antenna. The maximum potential energy (Uy) of the 50 nm EV is higher than that of the 30 nm EV by a factor of \sim 3.2. The simulation results also predict a slightly lower trapping stability along the y-direction in comparison to the result along the x direction, which is in agreement with the experimental results discussed in the next section. Figure 3D and Figure 3G show the calculated optical force and trapping potential energy along the z-axis. The particle is swept from 5 nm above the anapole antenna to 250 nm from the anapole antenna surface. Fz decays as the particle moves away from the hotspot, and both Fz and Uz become negligible when the z position of the EV is larger than 100 nm, which means that the trapped particle should be confined within a close distance to the surface of the anapole disk.

We performed trapping experiments to demonstrate anapole-assisted optical trapping using fluorescently labeled nanoscale EVs and supermere nanoparticle samples, as shown in Supporting Information Videos 1 and 2. The procedure for sample and particle preparation of EVs and supermeres is provided in the Supporting Information, sections S10 and S12. Figure 4A shows the sequence of frames describing the EV diffusing, trapping, and releasing. The linearly polarized laser is focused on the anapole disk, the EV diffuses to the vicinity of the anapole antenna, and it finally gets loaded onto the trap by the near-field optical force generated by the anapole antenna. It is worth mentioning that

across a wide range of incident angles, a focused light is capable of exciting the anapole mode.³⁷ After the EV is trapped, we tune the laser power to investigate the trapping stability as a function of the laser power. The particle tracking analysis is described in the Supporting Information, section S11. The scatter plot of the EV's position is shown in Figure 4B, indicating tighter trapping stability under higher laser power of 10.8 mW in comparison to a laser power of 6.8 mW. The EVs are mostly confined at the center under the 10.8 mW laser illumination, and the confinement becomes looser when the laser power is reduced from 10.8 to 6.8 mW. The extracted stiffness at 10.8 mW laser power along the x and y directions are 0.347 fN/nm and 0.329 fN/nm, respectively, after correcting for motion blur. To acquire trapping stiffness, we used the equipartition theorem approach while correcting for motion blur. 38,39 We first perform Gaussian fitting to estimate the variances $\langle x^2 \rangle$ and $\langle y^2 \rangle$ from the extracted particle displacements, and the stiffness in the x-direction (κ_x) is calculated using $\frac{1}{2}k_{\rm B}T = \frac{1}{2}\kappa_{\rm x}\langle x^2 \rangle$. To take into account the effect of motion blur, we employ a correction function as described in ref 39 and section S9 in the Supporting Information. Experiments were also performed to trap fluorescently labeled supermere samples as shown in Figure 4C. The same operations are performed during supermere trapping, as for EVs, and we also examine the trapping stability versus laser power. Figure 4D shows a scatter plot depicting the distribution of a trapped supermere's position in the anapole trap. The x and y positions of trapped supermere are expressed in histograms as shown in Figure 4E,F. The full

width at half-maximum (fwhm) obtained from the Gaussian fitted curve of the histogram was used to calculate the stiffness, and the correction function was applied to correct for the effect of motion blur. The stiffness under 19 mW laser power along the x and y directions are estimated as 0.215 fN/nm and 0.205 fN/nm, respectively. In order to confirm that the trapping of supermere is facilitated by the near field generated by the anapole resonator, we conducted experiments in which we rotated the polarization of the laser. Specifically, we defined the polarization along the x-axis as an angle of 0° and this angle would provide the best trapping stability under near-field trapping conditions. We predicted that at any other polarization angle, the trapping stability would degrade from this optimum angle. By contrast, laser trapping without the influence of the anapole state was expected to provide constant trapping stability regardless of the polarization angle.

To test these predictions, we changed the polarization angle from 0° to 20° and then to 40° from the x-axis, as shown in Figure 5A and Supporting Information Video 3. We observed that the trapping stability decreased as the polarization angle deviated from 0°, confirming the near-field trapping enabled by the anapole state. Specifically, when the polarization angle was set to 40°, the trapped particle showed a looser confinement and the displacements of the trapped particle appear to have an elliptical distribution that can be represented by a major and minor axis as depicted by the blue and red dotted arrows in Figure 5B. We performed numerical calculations to clarify this observation. Our findings indicate that as the laser's polarization shifts from 0°, the electric field enhancement in the DNH decreases. The decreased electric field enhancement results in a weakened trapping force acting on the particle, thereby leading to a reduced confinement of the particle's trajectory. The intensity distribution at 5 nm above the structure shown in Figure 5C indicates a distorted field with an intensity enhancement of approximately 260 times.

Based on our observations and calculations, we plotted the calculated trapping potentials along the minor axis and major axis, as indicated by the red and blue arrows in Figure 5C,D,E. These lines suggest that the potential along the major axis was lower than that along the minor axis, which is consistent with our observation in Figure 5B. In summary, our experimental results confirm that the observed stable trapping of supermeres and EVs is enabled by the enhanced near field generated by the anapole antenna rather than by the laser light itself.

In this study, we have demonstrated the ability to trap nanoscale EVs and the newly discovered supermeres using the nanoscale confined light fields enabled by optical anapole states for the first time. We achieved the stable trapping of supermeres with 2 orders of magnitude lower power relative to the trapping powers used in optical tweezers. The use of a Bragg reflector to control the reflection phase of the incident light and optimize field enhancement in the anapole structure instead of metallic films ensures that there is no loss-induced heating. Since the proposed trapping system is low-loss, it precludes local temperature rises and thus ensures that important biological particles and molecules remain intact. The absence of loss-induced heating also ensures that our system achieves low-power trapping of nanosized EVPs with high stability, without external thermohydrodynamic phenomena such as convection or thermophoresis that could interfere with trapping. Beyond optical trapping, this all-dielectric approach for optimizing and enhancing electromagnetic fields in all-dielectric systems may find applications in other areas

including low-threshold lasing and the enhancement of nonlinearities where high field enhancement with low loss is beneficial. In conclusion, our findings depict that the proposed anapole-assisted optical trapping is a promising approach for trapping and analyzing nanoscale biological particles and could have a wide range of applications in the future.

ASSOCIATED CONTENT

Solution Supporting Information

The Supporting Information is available free of charge at https://pubs.acs.org/doi/10.1021/acs.nanolett.3c02014.

Video 1 showing EV trapping with varying the incident power (MP4)

Video 2 showing supermeres trapping with varying the incident power (MP4)

Video 3 showing supermeres trapping with varying the polarization direction (MP4)

Reflectivity of DBR with varying the number of Si and SiO_2 pairs; The electric field enhancement depending on the thickness of space layer; radius sweep of Si nanoantenna; COMSOL modeling for thermal simulation; electric field distribution with varying the center-to-center of DNH; dark-field measurement setup; ellipsometry result of amorphous silicon; Maxwell's stress tensor (MST) calculation; correction function for motion blur; fabrication procedure; particle tracking method; sample preparation (PDF)

AUTHOR INFORMATION

Corresponding Author

Justus C. Ndukaife — Vanderbilt Institute of Nanoscale Science and Engineering, Vanderbilt University, Nashville, Tennessee 37235, United States; Department of Electrical and Computer Engineering, Department of Mechanical Engineering, and Center for Extracellular Vesicles Research, Vanderbilt University, Nashville, Tennessee 37235, United States; Orcid.org/0000-0002-8524-0657; Email: justus.ndukaife@vanderbilt.edu

Authors

Ikjun Hong – Vanderbilt Institute of Nanoscale Science and Engineering, Vanderbilt University, Nashville, Tennessee 37235, United States; Department of Electrical and Computer Engineering, Vanderbilt University, Nashville, Tennessee 37235, United States; orcid.org/0000-0003-1275-7740

Chuchuan Hong – Vanderbilt Institute of Nanoscale Science and Engineering, Vanderbilt University, Nashville, Tennessee 37235, United States; Department of Electrical and Computer Engineering, Vanderbilt University, Nashville, Tennessee 37235, United States; orcid.org/0000-0002-1329-9385

Oleg S. Tutanov — Department of Medicine, Vanderbilt University Medical Center, Nashville, Tennessee 37232, United States; Center for Extracellular Vesicles Research, Vanderbilt University, Nashville, Tennessee 37235, United States

Clark Massick — Department of Medicine, Vanderbilt University Medical Center, Nashville, Tennessee 37232, United States; Center for Extracellular Vesicles Research, Vanderbilt University, Nashville, Tennessee 37235, United States; Occid.org/0009-0009-4418-2006

- Mark Castleberry Department of Medicine, Vanderbilt University Medical Center, Nashville, Tennessee 37232, United States; Center for Extracellular Vesicles Research, Vanderbilt University, Nashville, Tennessee 37235, United States
- Qin Zhang Department of Medicine, Vanderbilt University Medical Center, Nashville, Tennessee 37232, United States; Center for Extracellular Vesicles Research, Vanderbilt University, Nashville, Tennessee 37235, United States
- Dennis K. Jeppesen Department of Medicine, Vanderbilt University Medical Center, Nashville, Tennessee 37232, United States; oorcid.org/0000-0002-7480-8083
- James N. Higginbotham Department of Medicine, Vanderbilt University Medical Center, Nashville, Tennessee 37232, United States; Center for Extracellular Vesicles Research, Vanderbilt University, Nashville, Tennessee 37235, United States
- Jeffrey L. Franklin Department of Medicine, Vanderbilt University Medical Center, Nashville, Tennessee 37232, United States; Department of Cell and Developmental Biology, Vanderbilt University, Nashville, Tennessee 37232, United States; Center for Extracellular Vesicles Research, Vanderbilt University, Nashville, Tennessee 37235, United States
- Kasey Vickers Department of Medicine, Vanderbilt University Medical Center, Nashville, Tennessee 37232, United States; Center for Extracellular Vesicles Research, Vanderbilt University, Nashville, Tennessee 37235, United States
- Robert J. Coffey Department of Medicine and Epithelial Biology Center, Vanderbilt University Medical Center, Nashville, Tennessee 37232, United States; Department of Cell and Developmental Biology, Vanderbilt University, Nashville, Tennessee 37232, United States

Complete contact information is available at: https://pubs.acs.org/10.1021/acs.nanolett.3c02014

Author Contributions

[¶]I.H. and C.H. contributed equally to this work.

Notes

The authors declare no competing financial interest.

ACKNOWLEDGMENTS

I.H., C.H., and J.C.N. acknowledge financial support from the National Science Foundation NSF CAREER Award (NSF ECCS 2143836). K.V. is supported by National Institutes of Health (Grant HL116263). R.J.C. is supported by Grants NIH/NCI R35CA197570, UH3CA241685, P01CA229123, and P50CA236733.

REFERENCES

(1) Volpe, G.; Maragò, O. M.; Rubinzstein-Dunlop, H.; Pesce, G.; Stilgoe, A. B.; Volpe, G.; Tkachenko, G.; Truong, V. G.; Chormaic, S. N.; Kalantarifard, F.; Elahi, P.; Käll, M.; Callegari, A.; Marqués, M. I.; Neves, A. A. R.; Moreira, W. L.; Fontes, A.; Cesar, C. L.; Saija, R.; Saidi, A.; Beck, P.; Eismann, J. S.; Banzer, P.; Fernandes, T. F. D.; Pedaci, F.; Bowen, W. P.; Vaippully, R.; Lokesh, M.; Roy, B.; Thalhammer, G.; Ritsch-Marte, M.; García, L. P.; Arzola, A. V.; Castillo, I. P.; Argun, A.; Muenker, T. M.; Vos, B. E.; Betz, T.; Cristiani, I.; Minzioni, P.; Reece, P. J.; Wang, F.; McGloin, D.; Ndukaife, J. C.; Quidant, R.; Roberts, R. P.; Laplane, C.; Volz, T.; Gordon, R.; Hanstorp, D.; Marmolejo, J. T.; Bruce, G. D.; Dholakia, K.; Li, T.; Brzobohatý, O.; Simpson, S. H.; Zemánek, P.; Ritort, F.;

- Roichman, Y.; Bobkova, V.; Wittkowski, R.; Denz, C.; Kumar, G. V. P.; Foti, A.; Donato, M. G.; Gucciardi, P. G.; Gardini, L.; Bianchi, G.; Kashchuk, A.; Capitanio, M.; Paterson, L.; Jones, P. H.; Berg-Sørensen, K.; Barooji, Y. F.; Oddershede, L. B.; Pouladian, P.; Preece, D.; Adiels, C. B.; De Luca, A. C.; Magazzù, A.; Ciriza, D. B.; Iati, M. A.; Swartzlander, G. A. Roadmap for Optical Tweezers. *arXiv* 2022, 2206.13789.
- (2) Kruglik, S. G.; Royo, F.; Guigner, J.-M.; Palomo, L.; Seksek, O.; Turpin, P.-Y.; Tatischeff, I.; Falcón-Pérez, J. M. Raman Tweezers Microspectroscopy of circa 100 Nm Extracellular Vesicles. *Nanoscale* **2019**, *11* (4), 1661–1679.
- (3) Penders, J.; Nagelkerke, A.; Cunnane, E. M.; Pedersen, S. V.; Pence, I. J.; Coombes, R. C.; Stevens, M. M. Single Particle Automated Raman Trapping Analysis of Breast Cancer Cell-Derived Extracellular Vesicles as Cancer Biomarkers. *ACS Nano* **2021**, *15* (11), 18192–18205.
- (4) Jeppesen, D. K.; Zhang, Q.; Franklin, J. L.; Coffey, R. J. Extracellular Vesicles and Nanoparticles: Emerging Complexities. *Trends Cell Biol.* **2023**, 33, 667–681.
- (5) Makarova, J.; Turchinovich, A.; Shkurnikov, M.; Tonevitsky, A. Extracellular MiRNAs and Cell-Cell Communication: Problems and Prospects. *Trends Biochem. Sci.* **2021**, *46* (8), 640–651.
- (6) Zhang, H.; Freitas, D.; Kim, H. S.; Fabijanic, K.; Li, Z.; Chen, H.; Mark, M. T.; Molina, H.; Martin, A. B.; Bojmar, L.; Fang, J.; Rampersaud, S.; Hoshino, A.; Matei, I.; Kenific, C. M.; Nakajima, M.; Mutvei, A. P.; Sansone, P.; Buehring, W.; Wang, H.; Jimenez, J. P.; Cohen-Gould, L.; Paknejad, N.; Brendel, M.; Manova-Todorova, K.; Magalhães, A.; Ferreira, J. A.; Osório, H.; Silva, A. M.; Massey, A.; Cubillos-Ruiz, J. R.; Galletti, G.; Giannakakou, P.; Cuervo, A. M.; Blenis, J.; Schwartz, R.; Brady, M. S.; Peinado, H.; Bromberg, J.; Matsui, H.; Reis, C. A.; Lyden, D. Identification of Distinct Nanoparticles and Subsets of Extracellular Vesicles by Asymmetric Flow Field-Flow Fractionation. Nat. Cell Biol. 2018, 20 (3), 332–343. (7) Zhang, Q.; Jeppesen, D. K.; Higginbotham, J. N.; Graves-Deal, R.; Trinh, V. Q.; Ramirez, M. A.; Sohn, Y.; Neininger, A. C.; Taneja, N.; McKinley, E. T.; Niitsu, H.; Cao, Z.; Evans, R.; Glass, S. E.; Ray, K. C.; Fissell, W. H.; Hill, S.; Rose, K. L.; Huh, W. J.; Washington, M. K.; Ayers, G. D.; Burnette, D. T.; Sharma, S.; Rome, L. H.; Franklin, J. L.; Lee, Y. A.; Liu, Q.; Coffey, R. J. Supermeres Are Functional
- (8) Wang, K.; Schonbrun, E.; Steinvurzel, P.; Crozier, K. B. Trapping and Rotating Nanoparticles Using a Plasmonic Nano-Tweezer with an Integrated Heat Sink. *Nat. Commun.* **2011**, 2 (1), 469.

Extracellular Nanoparticles Replete with Disease Biomarkers and Therapeutic Targets. Nature Cell Biology 2022 23:12 2021, 23 (12),

- (9) Juan, M. L.; Gordon, R.; Pang, Y.; Eftekhari, F.; Quidant, R. Self-Induced Back-Action Optical Trapping of Dielectric Nanoparticles. *Nat. Phys.* **2009**, *5* (12), 915–919.
- (10) Roxworthy, B. J.; Ko, K. D.; Kumar, A.; Fung, K. H.; Chow, E. K. C.; Liu, G. L.; Fang, N. X.; Toussaint, K. C. Application of Plasmonic Bowtie Nanoantenna Arrays for Optical Trapping, Stacking, and Sorting. *Nano Lett.* **2012**, *12* (2), 796–801.
- (11) Ghosh, S.; Ghosh, A. All Optical Dynamic Nanomanipulation with Active Colloidal Tweezers. *Nat. Commun.* **2019**, *10* (1), 4191.
- (12) Saleh, A. A. E.; Dionne, J. A. Toward Efficient Optical Trapping of Sub-10-Nm Particles with Coaxial Plasmonic Apertures. *Nano Lett.* **2012**, *12* (11), 5581–5586.
- (13) Crozier, K. B. Quo Vadis, Plasmonic Optical Tweezers? *Light: Sci. Appl.* **2019**, *8* (1), 35.
- (14) Juan, M. L.; Righini, M.; Quidant, R. Plasmon Nano-Optical Tweezers. *Nat. Photonics* **2011**, *5* (6), 349–356.
- (15) Baffou, G.; Girard, C.; Quidant, R. Mapping Heat Origin in Plasmonic Structures. *Phys. Rev. Lett.* **2010**, *104* (13), 136805.
- (16) Hong, C.; Yang, S.; Ndukaife, J. C. Optofluidic Control Using Plasmonic TiN Bowtie Nanoantenna. *Opt Mater. Express* **2019**, 9 (3), 953.
- (17) Hong, C.; Yang, S.; Kravchenko, I.; Ndukaife, J. C. Electrothermoplasmonic Trapping and Dynamic Manipulation of

Nano Letters pubs.acs.org/NanoLett Letter

- Single Colloidal Nanodiamond. Nano Lett. 2021, 21 (12), 4921–4927.
- (18) Xu, Z.; Song, W.; Crozier, K. B. Optical Trapping of Nanoparticles Using All-Silicon Nanoantennas. *ACS Photonics* **2018**, 5 (12), 4993–5001.
- (19) Jiang, Q.; Rogez, B.; Claude, J.-B.; Baffou, G.; Wenger, J. Quantifying the Role of the Surfactant and the Thermophoretic Force in Plasmonic Nano-Optical Trapping. *Nano Lett.* **2020**, *20* (12), 8811–8817.
- (20) Gargiulo, J.; Brick, T.; Violi, I. L.; Herrera, F. C.; Shibanuma, T.; Albella, P.; Requejo, F. G.; Cortés, E.; Maier, S. A.; Stefani, F. D. Understanding and Reducing Photothermal Forces for the Fabrication of Au Nanoparticle Dimers by Optical Printing. *Nano Lett.* **2017**, 17 (9), 5747–5755.
- (21) Yang, S.; Hong, C.; Jiang, Y.; Ndukaife, J. C. Nanoparticle Trapping in a Quasi-BIC System. ACS Photonics 2021, 8 (7), 1961–1971.
- (22) Gurvitz, E. A.; Ladutenko, K. S.; Dergachev, P. A.; Evlyukhin, A. B.; Miroshnichenko, A. E.; Shalin, A. S. The High-Order Toroidal Moments and Anapole States in All-Dielectric Photonics. *Laser Photon Rev.* **2019**, *13* (5), 1800266.
- (23) Miroshnichenko, A. E.; Evlyukhin, A. B.; Yu, Y. F.; Bakker, R. M.; Chipouline, A.; Kuznetsov, A. I.; Luk'yanchuk, B.; Chichkov, B. N.; Kivshar, Y. S. Nonradiating Anapole Modes in Dielectric Nanoparticles. *Nat. Commun.* **2015**, *6* (1), 8069.
- (24) Baryshnikova, K. V.; Smirnova, D. A.; Luk'yanchuk, B. S.; Kivshar, Y. S. Optical Anapoles: Concepts and Applications. *Adv. Opt Mater.* **2019**, *7* (14), 1801350.
- (25) Savinov, V.; Papasimakis, N.; Tsai, D. P.; Zheludev, N. I. Optical Anapoles. *Commun. Phys.* **2019**, 2 (1), 69.
- (26) Totero Gongora, J. S.; Miroshnichenko, A. E.; Kivshar, Y. S.; Fratalocchi, A. Anapole Nanolasers for Mode-Locking and Ultrafast Pulse Generation. *Nat. Commun.* **2017**, 8 (1), 15535.
- (27) Li, Y.; Huang, Z.; Sui, Z.; Chen, H.; Zhang, X.; Huang, W.; Guan, H.; Qiu, W.; Dong, J.; Zhu, W.; Yu, J.; Lu, H.; Chen, Z. Optical Anapole Mode in Nanostructured Lithium Niobate for Enhancing Second Harmonic Generation. *Nanophotonics* **2020**, *9* (11), 3575–3585
- (28) Jiang, Y.; Hong, C.; Yang, S.; Ndukaife, J. C.All-Dielectric Nanoantenna for Low Power Optical Trapping of Nanoscale Objects with Ultra-Low Heat Generation. 2021 Conference on Lasers and Electro-Optics, CLEO 2021—Proceedings; Optica Publishing Group, 2021; DOI: 10.1364/cleo qels.2021.fw3m.4.
- (29) Hernández-Sarria, J. J.; Oliveira, O. N.; Mejía-Salazar, J. R. Toward Lossless Infrared Optical Trapping of Small Nanoparticles Using Nonradiative Anapole Modes. *Phys. Rev. Lett.* **2021**, *127* (18), 186803.
- (30) Conteduca, D.; Brunetti, G.; Pitruzzello, G.; Tragni, F.; Dholakia, K.; Krauss, T. F.; Ciminelli, C. Exploring the Limit of Multiplexed Near-Field Optical Trapping. *ACS Photonics* **2021**, 8 (7), 2060–2066.
- (31) Jazayeri, A. M.; Mehrany, K. All-Dielectric Structure for Trapping Nanoparticles via Light Funneling and Nanofocusing. *JOSA B* **2017**, 34 (10), 2179–2184.
- (32) Xu, Z.; Song, W.; Crozier, K. B. Optical Trapping of Nanoparticles Using All-Silicon Nanoantennas. *ACS Photonics* **2018**, 5 (12), 4993–5001.
- (33) Querry, M. R.; Hale, G. M. Optical Constants of Water in the 200-Nm to 200-Mm Wavelength Region. *Appl. Opt.* **1973**, *12* (3), 555–563.
- (34) Jackson, J. D. Classical Electrodynamics, 3rd ed.; Wiley: New York, 1999; p 261.
- (35) Théry, C.; Witwer, K. W.; Aikawa, E.; Alcaraz, M. J.; Anderson, J. D.; Andriantsitohaina, R.; Antoniou, A.; Arab, T.; Archer, F.; Atkin-Smith, G. K.; et al. Minimal Information for Studies of Extracellular Vesicles 2018 (MISEV2018): A Position Statement of the International Society for Extracellular Vesicles and Update of the MISEV2014 Guidelines. J. Extracell Vesicles 2018, 7 (1), 1535750.

- (36) Gardiner, C.; Shaw, M.; Hole, P.; Smith, J.; Tannetta, D.; Redman; Ian, C. W.; Sargent, L. L. Measurement of Refractive Index by Nanoparticle Tracking Analysis Reveals Heterogeneity in Extracellular Vesicles. *J. Extracell. Vesicles* **2014**, 3 (1), 25361.
- (37) Miroshnichenko, A. E.; Evlyukhin, A. B.; Yu, Y. F.; Bakker, R. M.; Chipouline, A.; Kuznetsov, A. I.; Luk'yanchuk, B.; Chichkov, B. N.; Kivshar, Y. S. Nonradiating Anapole Modes in Dielectric Nanoparticles. *Nat. Commun.* **2015**, *6* (1), 8069.
- (38) Sarshar, M.; Wong, W. T.; Anvari, B. Comparative Study of Methods to Calibrate the Stiffness of a Single-Beam Gradient-Force Optical Tweezers over Various Laser Trapping Powers. *J. Biomed Opt* **2014**, *19* (11), 115001.
- (39) Wong, W. P.; Halvorsen, K. The Effect of Integration Time on Fluctuation Measurements: Calibrating an Optical Trap in the Presence of Motion Blur. *Opt. Express* **2006**, *14* (25), 12517–12531.